Influence of steam addition and elevated ambient conditions on NO_x reduction in a staged premixed swirling NH_3/H_2 flame

Daniel Pugh*, Philip Bowen, Agustin Valera-Medina, Anthony Giles, Jon Runyon, Richard Marsh

Cardiff School of Engineering, Cardiff University, Wales CF24 3AA, UK

Abstract

There is growing interest in the application of renewably-generated NH_3 to support future energy require-ments, however combustor designs and strategies require considerable development to reduce NO_x emissions in particular. A turbulent swirl burner was used to experimentally and numerically appraise potential path-ways for operational NO_x reduction with a premixed NH_3/H_2/air flame. Reactants were supplied at elevated temperature with parametric changes made to pressure and humidity. Favourable agreement was demon-strated between exhaust gas measurements and chemical kinetic simulations with a reactor network model, showing NO_x emissions to be sensitive to operational equivalence ratio, increasing by several orders of mag-nitude across the experimental range. The lowest NO_x concentrations were achieved at the richest conditions, accompanied by high unburned fuel fractions in the product stream. An increase in combustor pressure re-markably reduced exhaust NO_x concentrations primarily due to enhanced NH_2 formation, and subsequent NO consumption in the post-flame zone. Reactant humidification was explored in detail for the first time with this fuel, and shown to reduce NO_x production limiting thermal pathways with the extended Zel'dovich mechanism. NO consumption in the post-flame zone was also enhanced through an increase in OH-produced NH_2, and together with pressure, resulted in elevated exhaust NH_3 concentrations. Whilst this effect was comparatively small, it meant that leaner humidified operation could be employed to reduce unburned fuel fractions without a NO_x penalty. Emissions performance was further improved by the application of staged combustion, with secondary airflow used to improve fuel burnout. Humidity and pressure were optimised in the staged configuration to achieve operation with sampled respective NO_x and NH_3 exhaust fractions of 32 and 50 ppmvd (15%O_2), at a globally lean equivalence ratio. There is considerable scope for further system optimisation through improved mixing of secondary air and increased ambient pressure.
© 2018 The Authors. Published by Elsevier Inc. on behalf of The Combustion Institute.
This is an open access article under the CC BY license. (http://creativecommons.org/licenses/by/4.0/)

Keywords: Ammonia; Turbulent premixed flames; Humidified combustion; Staged combustion; Chemical kinetics

---

* Corresponding author.
E-mail address: pughdg@cardiff.ac.uk (D. Pugh).

1. Introduction

There is increasing interest in the application of renewably-generated NH_3 to support future energy requirements primarily due to its favourable transportation and storage characteristics [1–2], with existing infrastructure particularly attractive for rapid deployment [3]. The potential exists to employ NH_3 directly as a fuel in modified power plants and avoid complete conversion back to hydrogen. However, there are several outstanding combustion challenges associated with the utilisation of NH_3, principally due to its low flame speed, temperature and reactivity, in addition to the huge potential for NO_x production [4–6]. Supplementary fuels such as H_2 have been shown to improve and stabilise operational performance [6–12]. Nevertheless, traditional combustor designs require fundamental appraisal and development to reduce NO_x emissions before NH_3 can realistically be considered for sustained use in relatively clean and efficient technologies, such as gas turbines [8–11].

1.1. Scope

The aim of this work was to experimentally and numerically appraise the application of an NH_3/H_2 blend in a premixed swirl combustor at elevated temperature and pressure, to investigate potential pathways for operational NO_x reduction. First, the change in emission formation is characterised for variation in equivalence ratio, with chemical kinetic processes simulated using a reactor network model. Change in operational NO_x concentrations are then studied in detail at elevated conditions, increasing combustor pressure with density-scaled flow. This is combined with the humidification of premixed reactants to investigate the effect of H_2O on NO_x formation for the first time with this fuel, whilst maintaining flame stability. Finally, the combustor is employed in a staged configuration to allow for the introduction of secondary air, similar to existing rich-burn, quick-quench, lean-burn ('RQL') systems [13] - which in typical applications operate at significantly higher pressures - with parametric changes in flow, humidity and pressure all explored with secondary airflow. Chemical kinetics influences are explored in detail with the empirical NH_3/H_2 flame and changes in pressure and humidity. The concepts investigated are combined to develop a combustor configuration that provides optimised emissions performance.

2. Experimental facility

Experiments were undertaken using a premixed swirl burner at Cardiff University's Gas Turbine Research Centre (GTRC) housed within an optical pressure casing, and modified from previous programs [14–15]. The burner and casing assembly are shown in Fig. 1. The instrumentation lance
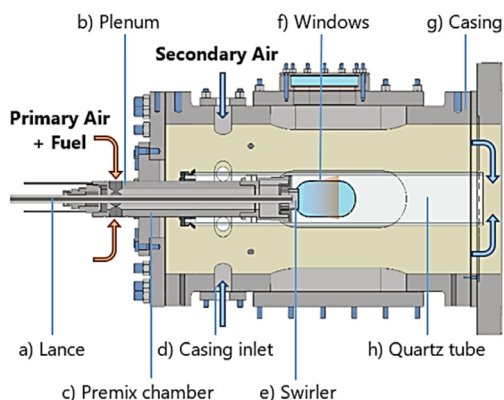

Fig. 1. Facility schematic.

(Fig. 1a) facilitates conditional measurements at the swirler outlet. Preheated reactants enter the inlet plenum (Fig. 1b), with mass-flowrates quantified using Coriolis meters ($\pm 0.35\%$). Gaseous NH_3 and H_2 were supplied independently from external storage, with air provided from a compressor (GA-45VSD), dried to a dew point of $-17°C$ (DPRA960). Steam was supplied using a heated line, with the burner conditioned to operational temperature using preheated air. Water supply was regulated using another scaled mass-flow controller ($\pm 0.2\%$) and vaporised in two heaters. After entering the plenum, reactants travel through the premix chamber (Fig. 1c) to a single radial-tangential swirler (Fig. 1e) and out through the burner exit nozzle (20 mm radius). The outlet has a geometric swirl number equivalent to $Sg = 0.8$. Optical access is afforded via quartz viewing windows (Fig. 1f) housed within the casing (Fig. 1g) with flame chemiluminescence imaged from above. The burner was operated with a cylindrical quartz confinement tube, at an expansion ratio of 2.5 from the burner nozzle exit (Fig. 1h). Secondary air for staged combustion is introduced through the casing inlet (Fig. 1d), flowing around the quartz tube. Additional transducers were installed to monitor operational parameters, with further detail provided elsewhere [14–15]. The system was pressurised using a water-cooled back-pressure valve with incremental control.

2.1. Chemiluminescence

The chemiluminescence of an excited hydroxyl (OH) radical has been used to provide a non-intrusive indication of localised heat release, and a generalised marker of flame front location [14–16]. The image plane is centered on the burner exit, with respective view fields of $\sim100/75$ mm in the radial and axial directions. For each experiment 200 images were captured at a rate of 10 Hz, with intensifier gain held constant. Intensities measured for

each dataset were background-corrected and averaged, with a false colourmap applied. As demonstrated in previous studies [14], the flow-field generated by the swirl configuration has been evaluated using particle image velocimetry [17], with the flame structure typical for a premixed swirler of this design: The outward flow generates a conical flame around a shear layer of zero axial velocity, and central recirculation zone (CRZ). A modified open-access Abel inversion algorithm [14] was used to transform the temporally-averaged images into planar representations of the OH* chemiluminescence intensity distribution. Detailed information regarding the image capture system and processing technique can be found elsewhere [14–15].

2.2. Emissions measurements

The emissions measurement system was designed in accordance with ISO-11,042 [18]. Exhaust products were sampled downstream of the quartz confinement using a multi-point equal area probe connected to a water-conditioned heat exchanger, used to regulate the sample temperature to 433 K. A heated pump was used to deliver products to the analysis suite, and was also maintained at 433 K together with the filter and sample lines. NO_x ($NO + NO_2$) concentrations were quantified using a heated vacuum chemiluminescence analyser (Signal 4000VM). The sample stream could be redirected through an NH_3 to NO converter (Signal 410) to measure unburned concentrations with an 80% conversion efficiency. All NO_x and NH_3 concentrations were measured hot/wet with captured data normalised to equivalent dry conditions (Eqn. (9) ISO-11,042 [18]).

Additional sample was dried in a chiller before O_2 concentration was quantified using a paramagnetic analyser (Signal 9000MGA). Dry measurements were subsequently normalised to equivalent 15% O_2 (Eqn. (10) ISO-11,042 [18]). Burner outputs were monitored after changing experimental set-points, and with temperatures stable, flows were held on condition and at least 60 samples taken. NO_x and NH_3 were measured separately, with richest test points requiring small amounts air dilution in the sample to provide O_2 for NH_3 conversion and measurement. NH_3 concentrations were corrected to account for this dilution prior to analysis. Measured uncertainties comprise analyser specification, linearisation and span gas certification. These were combined with fluctuations in measurement to give a total uncertainty represented by the plotted error bars.

3. Experimental specification

A fuel blend with an NH_3/H_2 ratio of 70/30%$_{mol}$ was specified for this program. Alternative ratios were appraised [11], with the chosen blend shown

Table 1
Summary of experimental conditions.

Ø	P_{1-4} (MPa)	WL_{1-4} (g·s^{-1})	SA_{1-3} (g·s^{-1})
1.2,	0.105	0, 0.2, 0.4, 0.6	0, 3, 6
1.25,	0.131	0, 0.25, 0.5, 0.75	0, 3.75, 7.5
1.3	0.158	0, 0.3, 0.6, 0.9	0, 4.5, 9
	0.184	0, 0.35, 0.7, 1.05	0, 3

to provide most stable performance between a susceptibility to flashback – apparent with excessive H_2 (> 40%) – and blowoff stability at richer conditions. This ratio has also been shown to behave analogous to a premixed CH_4 flame [8], with the employed burner characterised extensively using CH_4/air mixtures [19]. A comprehensive test matrix was specified and only the most significant results are presented and discussed, with the full dataset available as supplementary material. Baseline conditions were specified at a thermal power of 25kW$_n$ with a combustor pressure of 0.105MPa$_a$ (P_1), no supplementary steam addition or secondary airflow. Equivalence ratios were calculated relative to the stoichiometric fuel-air ratio of the NH_3/H_2 blend (Ø = fuel-air/fuel-air$_{stoich}$ from $0.3H_2 + 0.7NH_3 + 0.675O_2 + 2.54N_2 \rightarrow 1.35H_2O + 2.89N_2$) and were initially trailed in the range Ø = 1-1.4, with values Ø = 1.2, 1.25, and 1.3 (airflows of 6.56, 6.30, and 6.06g s^{-1}) selected for detailed parametric study with independent changes in humidity, pressure, and secondary airflow.

Steam was introduced at four distinct humidified fractions: $WL_1 = 0$, $WL_2 = 0.2$, $WL_3 = 0.4$ and $WL_4 = 0.6$g s^{-1} corresponding to overall reactant fractions of 0, 3.43, 6.63, and 9.63%$_{mol}$ at Ø = 1.2, which rise marginally with Ø due to the drop in airflow. Secondary air loadings for staged combustion were specified at ~50% and ~100% of the baseline combustor airflow ($SA_1 = 0$, $SA_2 = 3$ and $SA_3 = 6$g s^{-1}). Pressure was increased across the range $P_1 = 0.105$, $P_2 = 0.131$, $P_3 = 0.158$ and $P_4 = 0.184$ MPa, with all given flow rates scaled with change in density to maintain equivalent nozzle exit velocities, and residence times in the combustor. The experimental specification is summarised in Table 1, with a detailed matrix outlining each condition provided in the supplemental material, alongside measured NO_x and NH_3 concentrations. The highest pressure specification was governed by the maximum sustainable NH_3 vapour flow of 1.8g s^{-1}, with current operation limited at this point. At higher flows, NH_3 expansion reduced the drum temperature to limit supply vapour pressure. Combustor inlet temperature was maintained at 423 ± 5 K.

3.1. Chemical kinetics modelling

Chemical kinetics was modelled for each experimental condition using CHEMKIN-PRO. The

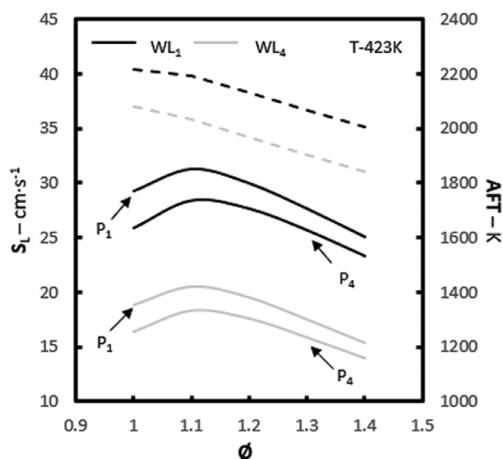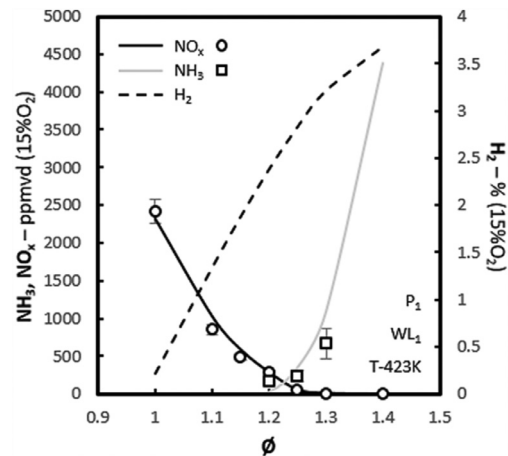Fig. 2. Modelled S_L (solid) and AFT (dotted) for the specified experimental range.

Fig. 3. Experimental (markers) and modelled (lines) NO_x NH_3 and H_2 concentrations against Ø at baseline conditions.

PREMIX reactor was initially used to provide 1-D simulations of changes in laminar flame speed (S_L). Solutions were based on an adaptive grid of 1000 points, with multi-component transport properties and trace species approximation. The equilibrium tool was used to generate adiabatic flame temperatures (AFT), under conditions of constant pressure and enthalpy. Each simulation employed the Tian et al. reaction mechanism [20] comprising 84 chemical species and 703 reactions, and optimised for use with NH_3 mixtures. Several other mechanisms were appraised [21–22], with the employed chemistry set providing the most favourable agreement with experimental data, alongside the reduced mechanism developed by Xiao et al. [22]. The predicted changes in S_L and AFT are shown for a range of Ø, with the highest pressures and H_2O loadings in Fig. 2 (changes in AFT with pressure are not shown as differences were negligible). At baseline conditions AFT is high enough to facilitate significant thermal NO_x formation [23], which is reduced by ~150 K with the maximum water loading, WL_4. However, this also causes a ~40% reduction in S_L, with this drop in reactivity signifying reduced flame stability, particularly at the richest conditions.

A hybrid reactor network model was developed to simulate the chemistry of the experimental swirling flame [10–11,24]. Three inlets were used to provide fuel, air and steam flows, with three perfectly stirred reactors (PSR) to model the pre-mixing, flame and central recirculation zones (20% recycled flow [25]). The outlet from the flame zone fed a Plug Flow Reactor (PFR) to simulate reactions in the post-flame zone. The model was setup with representative combustor geometry, with residence times calculated from empirical flow conditions. Reactor temperature was defined from equilibrium conditions, with flame temperature

calculated by the model, and set-points in the post-flame zone obtained from experimental results and system geometry. Heat loss was estimated to be 10%, with initial values compared to empirical results at baseline conditions to give favourable agreement with sampled concentrations. It should be emphasised that moderate uncertainty is associated with reactor networks, and the developed model was primarily used for empirical analysis, as opposed to prediction. Conditions were scaled with pressure, with all other geometric variables held constant, and only flowrates changed for each experimental set-point to give the plotted results. Plotted results from each modelled condition represent the combined $NO + NO_2$ fractions, equivalent to the measurements taken with the analyser described in Section 2.2. Each input variable can be found alongside unmeasured additional concentrations predicted by the model in the supplemental material.

4. Results

At baseline conditions of pressure and water loading the range of experimental Ø was broadened from 1-1.4, with sampled NO_x concentrations plotted alongside modelled results in Fig. 3 (NH_3 data were only captured across the original specified range). Good agreement is noted between the sampled NO_x concentrations and modelled predictions (both normalised to equivalent conditions), with slightly greater discrepancy for the NH_3 data. Low NO_x concentrations achievable with rich mixtures have been shown by other researchers [12], but operation at such conditions incurs an efficiency drop due to unburned fuel. NO_x reduction is achieved through a combination of reduced
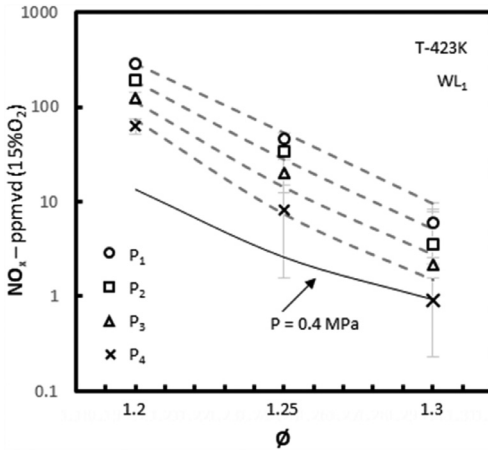
Fig. 4. Experimental (markers) and modelled (lines) NO_x concentrations against Ø at elevated pressure.

Fig. 5. Experimental (markers) and modelled (lines) NH_3 concentrations against Ø at elevated pressure.

thermal formation with the Zel'dovich mechanism [23] in the flame zone and NO consumption in the post-flame zone. Modelled inlet temperatures were increased to 515 K for the Ø = 1.3 condition (giving a near equivalent AFT to that at Ø = 1.2), with this thermal effect shown to approximately double the NO_x product fraction, but still amounting to < 10% of the original Ø = 1.2 case. The relative increase in NH_3 at richer Ø also leads to a significant increase in NH_2 in the post-flame zone, which enhances NO consumption through the chain carrying reaction $NH_2 + NO \leftrightarrow NNH + OH$ and the terminating reaction $NH_2 + NO \leftrightarrow H_2O + N_2$. The range of experimental Ø was restricted to Ø = 1.2-1.3 for further experiments to focus on the configuration that generated favourable NO_x concentrations (< 500ppmvd), without excess unburned H_2 and/or NH_3.

4.1. Elevated pressure

The influence of moderately elevated pressure was explored in the specified range up to 0.185 MPa (P_4), with operation at higher pressures requiring a fuel pre-heating vaporiser. Sampled NO_x concentrations were nevertheless reduced by a near order of magnitude across the experimental range, as shown in Fig. 4 (experimental markers are superimposed on the corresponding model prediction). This reduction is predicted to diminish as pressure is increased further, as demonstrated with modelled data at 0.4 MPa represented by the solid line, but suggests implementation at increased pressure could allow for leaner operation. An increase in pressure was also predicted to give a rise in unburned NH_3 concentration, with experimental trends broadly agreeing, as demonstrated in Fig. 5. NH_3 data could not be captured at P_4 due to experimental runtime limitations.
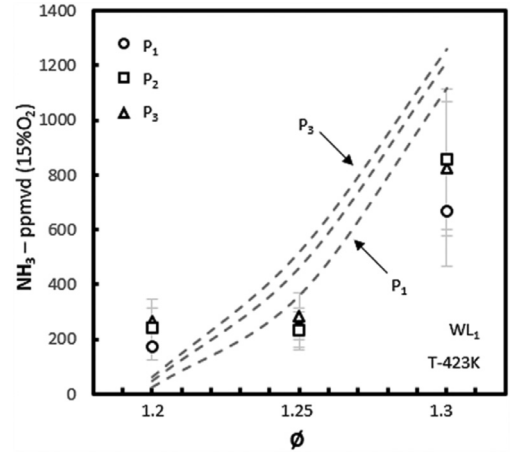
This influence of elevated pressure has recently been investigated numerically by Somarathne et al. [26] up to 0.5 MPa with swirling NH_3/air flames, following work from Valera-Medina et al. [10] with CH_4/NH_3/air. The predicted reduction in NO_x formation with pressure from the numerical NH_3/air flame is small compared to the experimental results presented in Fig. 4. This was attributed [26] to the influence of OH in NH_2 oxidation, alongside the role of HNO in NO production, and used to explain why results demonstrated a reduced influence at Ø = 1.25. By contrast, a near equivalent fractional offset in NO_x reduction is evident between the model and experiments, across the range of Ø for NH_3/H_2/air flames presented here. Hayakawa et al. [27] demonstrated equivalent trends for reduced NO_x production with increased pressure, however the measured concentrations were significantly lower than those expected at Ø = 1 when compared to this and other work [12]. This may have resulted from the removal of H_2O from the sampled gas stream and the indeterminate H_2 fraction used to stabilise a pilot flame - the influence of H_2 fraction was numerically investigated in this work, with an increase in H_2/NH_3 ratio shown to reduce the observed effect for NO_x reduction with increased pressure. To enhance the kinetic analysis still further, Fig. 6 shows a comparison between the absolute rates of NO fractions produced from prominent reactions in both the flame zone PSR, and at a fixed axial distance (0.01 m) in the post-flame zone with changes in ambient pressure. The results identify an increase in reactions governing NO production as pressure rises in the flame zone (Fig. 6a). This is offset by near equivalent increases in NO consumption mechanisms, ultimately leading to a marginal reduction (∼5%) in NO fraction in the flame zone. However, NH and NH_2 become more significant as NO is consumed in the post-flame
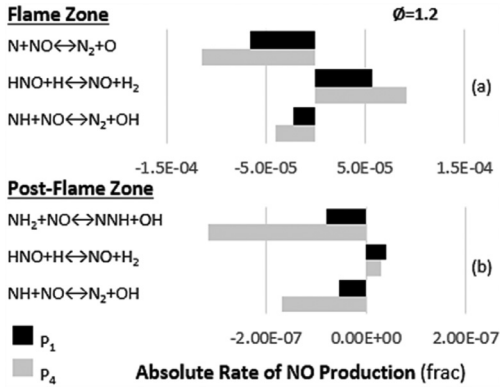
Fig. 6. Comparison between absolute rates of NO production from selected reactions at elevated pressure.
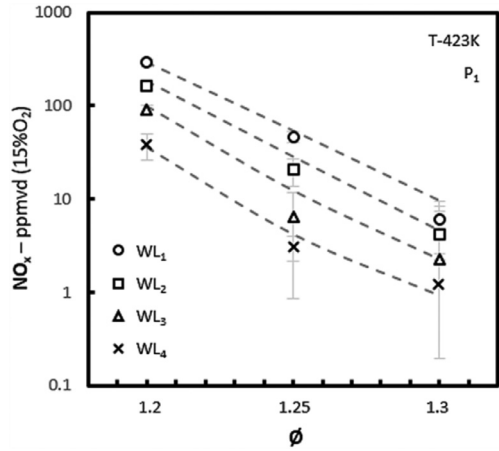

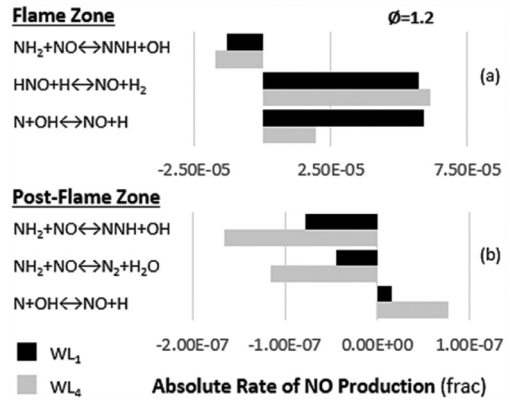Fig. 7. Experimental (markers) and modelled (lines) NO_x concentrations against Ø with increased humidification.

Fig. 8. Comparison between absolute rates of NO production from selected reactions with increased humidification.

zone (Fig. 6b), as rates from the shown mechanisms increase with pressure. This results from enhanced OH consumption and the production of NH_2 from $NH_3 + OH \leftrightarrow NH_2 + H_2O$, which also leads to the formation of more NH through chain carrying mechanisms with OH and H. NO production rates also decrease from $HNO + H \leftrightarrow NO + H_2$, and whilst there is a relative increase through mechanisms such as $NH + NO \leftrightarrow N_2O + H$ and $N + OH \leftrightarrow NO + H$, fractions are diminished with overall NO consumption. Similar influences are evident at Ø = 1.3, with a small reduction in NO formation in the flame zone, and enhanced consumption downstream, with the third body reaction $NO + H(+ M) \leftrightarrow HNO(+ M)$ shown to be more prominent. The increase in unburned NH_3 primarily results from elevated NH_2 concentrations, with reactions $2NH_2 \leftrightarrow NH_3 + NH$ and $NH_2 + H + M \leftrightarrow NH_3 + M$; however this influence is small compared to relative NO_x reduction.

4.2. Reactant humidification

Reactant humidification is an effective process for controlling NO_x through the combined influences of reduced flame temperature, alongside enhanced O consumption through the reaction $O + H_2O \leftrightarrow OH + OH$, to limit $N_2 + O \leftrightarrow NO + N$ [23]. In this work, the efficacy of employing humidification for NO_x reduction has been studied with fuel-bound nitrogen in NH_3, increasing H_2O fraction to $\sim 10\%_{mol}$ at WL_4. Beyond this concentration at Ø = 1.3 the flame began to appear unstable, flickering with intermittent detachment from the burner. Results are plotted against change in Ø for each water loading at P_1 in Fig. 7, again with experimental markers superimposed on each corresponding modelled line.

Again, favourable agreement was observed between the model and experiments, with H_2O loading shown to reduce product NO_x fraction by around an order of magnitude across the spec-

ified range. Alongside the expected reduction in $N_2 + O \leftrightarrow NO + N$, temperature drop ($\sim 150\,K$ at WL_4) in the flame zone inhibited NO production rate from the reaction $N + OH \leftrightarrow NO + H$, with Fig. 8a showing the water loading comparison for Ø = 1.2. Models also suggest a relative rise in NO consumption through NH_2 mechanisms, resulting from enhanced NH_3 decomposition, offset against an increase from $HNO + H \leftrightarrow NO + H_2$. Nevertheless, H_2O addition ultimately leads to a greater relative decrease in flame zone NO fraction. Enhanced NO consumption in the post-flame zone (0.01 m) results from similar mechanisms to those shown for an increase in pressure, reacting with NH_2 through the reactions discussed in Section 4.1 (Fig. 8b), albeit by a reduced amount. However, elevated OH concentrations (from H_2O) react to provide increased NO production through $N + OH \leftrightarrow NO + H$, counteracting the enhanced
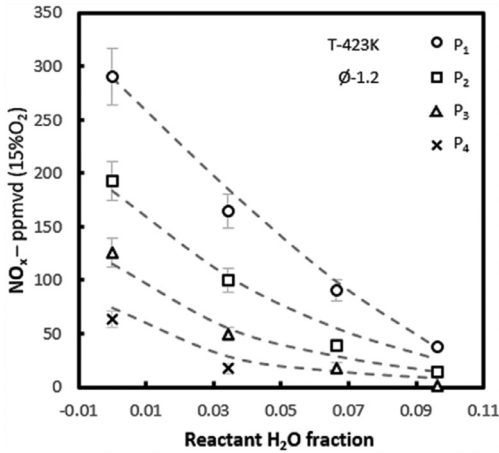
Fig. 9. Experimental (markers) and modelled (lines) NO_x concentrations against reactant water fraction with increased pressure ($\emptyset = 1.2$).

Fig. 10. Average raw (a) and Abel deconvoluted (b) OH^* chemiluminescence for varying $\emptyset$ and secondary airflow.

consumption. Again, elevated NH_2 concentrations provide an increase in unburned NH_3, with values marginally higher than those measured from a rise in pressure (Fig. 5).

Due to differences in the mechanisms governing NO_x formation, the influences of pressure and H_2O can be combined to provide a greater overall reduction, as shown for $\emptyset = 1.2$ in Fig. 9 (similar trends were observed for $\emptyset = 1.25$ and 1.3), again with measurements superimposed onto modelled data. The reduction in flame zone NO from H_2O addition is coupled with enhanced consumption at pressure to reduce production in the post-flame zone. It should be emphasised that whilst the combined influences of pressure and H_2O both cause an increase in unburned NH_3, when offset against a change in $\emptyset$, the net effect is still a reduction (Fig. 5). Hence leaner operational $\emptyset$ can be employed to reduce unburned fuel fractions without a NO_x penalty. This is particularly significant for gas turbine combustion, where the introduction of H_2O could also be achieved through an exhaust gas recirculation (EGR) configuration, to control operational combustor temperatures.

4.3. Staged combustion

In an attempt to reduce unburnt NH_3 whilst retaining good NO_x performance, the burner was reconfigured for staged combustion, with secondary air supplied around the quartz tube to form a supplementary downstream reaction zone. It was important to ensure the additional airflow did not dilute the primary flame, due to the demonstrated sensitivity of NO_x to change in $\emptyset$. OH^* chemiluminescence was used to validate the experimental technique, with Fig. 10 showing the difference between $\emptyset = 1.2$ and $\emptyset = 1.3$ with
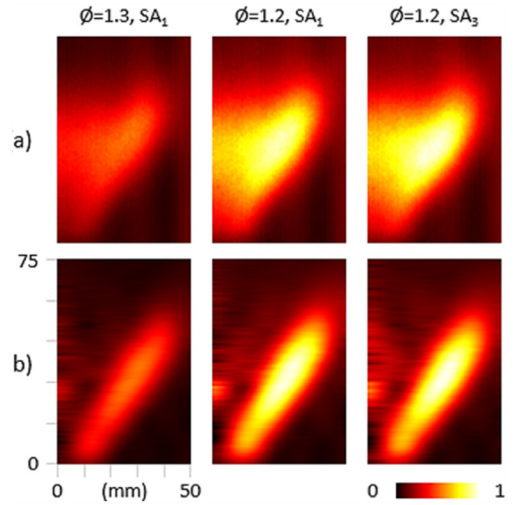
no secondary air, alongside an equivalent flame at SA_3. The secondary reaction zone is not visible in the optical window (Fig. 1f). Half-flames are shown ($x = 0$ mm on the burner centreline) with the captured 200 image average (Fig. 10a) provided above Abel deconvoluted planar representations (Fig. 10b), and colourmap normalised to the equivalent intensity distribution. Minimal differences were observed, and integral intensity values (II_{OH^*}, following Runyon [19]) were obtained, giving an average difference of $\sim 4\%$ with all secondary airflows, compared to a measured increase of $\sim 56\%$ from $\emptyset = 1.3$ to $\emptyset = 1.2$.

Increasing secondary airflow to SA_2 reduced the global $\emptyset$ (calculated using combined combustion and secondary air) to 0.82–0.87 (change in primary flame denoted by $\emptyset_p = 1.2–1.3$) to improve fuel burnout efficiency, where substantially higher fully premixed NO_x concentrations would be expected [12]. Measured NO_x values are plotted against change in water loading at P_1 (empty) and P_3 (shaded) in Fig. 11. A PSR reactor was insufficient for modelling this secondary flame with poor correlation obtained unsurprisingly, instead empirical trendlines for each experimental P_1 are superimposed. Contrasting tendencies are observed for a change in water loading, with a significant reduction observed at $\emptyset_p = 1.2$, compared to a marginal increase at $\emptyset_p = 1.3$. It is suggested that this results from the influence of H_2O on the change in primary NO_x concentration, offset against an increase in unburned NH_3. Minimal NO_x produced in the primary flame at $\emptyset_p = 1.3$ means formation mostly results from unburned NH_3 at the tube outlet, which increases with H_2O loading. This explanation is supported by the relative increase also observed with rising pressure.
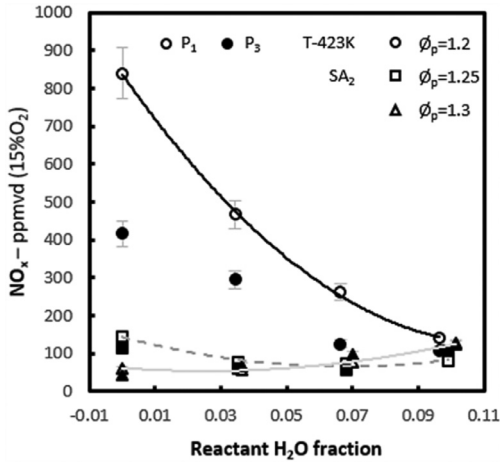
Fig. 11. Experimental NO_x concentrations against reactant water fraction with increased pressure and secondary airflow.
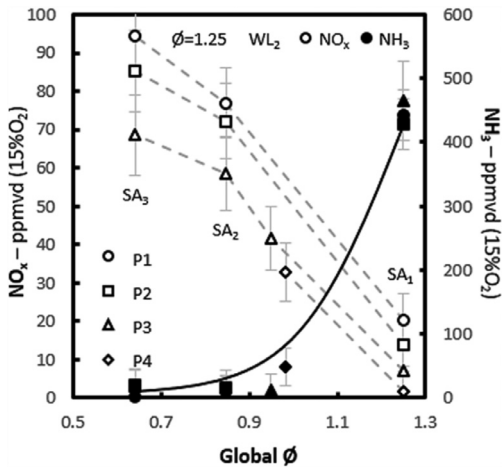

Fig. 12. Experimental NO_x (open) and NH_3 (shaded) concentrations against global Ø with increased pressure and secondary airflow.

Measured NO_x concentrations were also sensitive to secondary air flowrate, with the change in normalised values (open markers, dotted trendlines) from the $Ø_p = 1.25$ flame plotted against global Ø in Fig. 12. Measured NH_3 fractions (shaded) are also included with trendlines superimposed for clarity. It is apparent that an optimal point can be selected where both NO_x and unburned NH_3 concentrations are minimised through careful choice of humidity, pressure, and secondary airflow. An operational point was specified at WL_2 and P_4, with secondary air increased to give a global Ø of 0.98, generating respectable product NO_x and NH_3 fractions of $\sim$32ppmvd(15%O_2) and $\sim$50ppmvd(15%O_2). The current burner design is simple, offering non-optimised mixing of the secondary airflow in particular. The facility is currently under development to enable enhanced mixture control with secondary humidity, and operation at significantly higher pressure.

5. Conclusions

The NO_x emissions produced by a premixed swirling NH_3/H_2 flame are sensitive to operational Ø, increasing by several orders of magnitude across the experimental range. NO_x concentrations < 10ppmvd can be achieved at the richest conditions, however this is accompanied by high fractions of unburned fuel and a corresponding reduction in combustion efficiency.

Consistent with recent model predictions for NH_3 flames, an increase in combustor pressure has been shown experimentally to lower exhaust NO_x concentrations for the first time. Chemical kinetic models suggest this primarily results from enhanced NH_2 formation, acting to consume NO in the post-flame zone. Unburned NH_3 concentrations are also produced from the reactive NH_2, however the influence is small compared to change in NO_x.

Reactant humidification reduces NO_x concentrations in the flame zone, limiting thermal production pathways with the extended Zel'dovich mechanism. NO consumption in the post-flame zone is also enhanced through an increase in OH-produced NH_2, and again results in higher unburned NH_3 concentrations. When offset against a change in Ø the net effect is still a reduction, meaning leaner operation can be employed to reduce unburned fuel fractions without incurring a NO_x penalty.

The emissions performance of an NH_3/H_2 swirling flame can be further improved by using a combination of humidity and secondary airflow in a staged configuration, and is enhanced by operation at elevated pressure. However, careful specification of equivalence ratio is required as excessive unburned NH_3 will eventually increase NO_x formation in the secondary reaction zone.

Supplementary materials

Supplementary material associated with this article can be found, in the online version, at doi:10.1016/j.proci.2018.07.091.

References

[1] C. Zamfirescu, I. Dincer, *J. Power Sources* 185 (1) (2008) 459–465.

[2] A. Karabeyoglu, B. Evans, J. Stevens, B. Cantwell, Development of ammonia based fuels for environmentally friendly power generation, *AIAA, paper AIAA2012-4055*, 2012.

[3] C.H. Christensen, T. Johannessen, R.Z. Sørensen, J.K. Nørskov, *Catal. Today* 111 (1) (2006) 140–144.

[4] U.J. Pfahl, M.C. Ross, J.E. Shepherd, K.O. Pasamehmetoglu, C. Unal, *Combust. Flame* 123 (2000) 140–158.

[5] A. Hayakawa, T. Goto, R. Mimoto, Y. Arakawa, T. Kudo, H. Kobayashi, *Fuel* 159 (2015) 98–106.

[6] O. Mathieu, E.L. Petersen, *Combust. Flame* 162 (2015) 554–570.

[7] H. Nozari, G. Karaca, O. Tuncer, A. Karabeyoglu, *Int. J. Hydrogen Energy* 42 (21) (2017) 14775–14785.

[8] F.J. Verkamp, M.C. Hardin, J.R. Williams, *Proc. Comb. Inst.* 11 (1) (1967) 985–992.

[9] O. Kurata, N. Takayuki, M. TakahiroInoue, T. Tsujimura, H. Furutani, H. Kobayashi, A. Hayakawa, *Proc. Comb. Inst.* 36 (3) (2017) 3351–3359.

[10] A. Valera-Medina, R. Marsh, J. Runyon, D. Pugh, P. Beasley, T. Hughes, P. Bowen, *Appl. Energy* 185 (2) (2017) 1362–1371.

[11] A. Valera-Medina, D. Pugh, R. Marsh, G. Bulat, P. Bowen, *Int. J. Hydrogen Energy* 42 (2017) 24495–24503.

[12] A. Hayakawa, Y Arakawa, R. Mimoto, K.D. Kunkuma, A. Somarathne, T. Kudo, H. Kobayashi, *Int. J. Hydrogen Energy* 42 (19) (2017) 14010–14018.

[13] A. Lefebvre, D. Ballal, Gas Turbine Combustion, CRC Press, FL, USA, 2010, p. 418.

[14] D. Pugh, P. Bowen, R. Marsh, A. Crayford, J. Runyon, S. Morris, A. Valera-Medina, A. Giles, *Combust. Flame* 177 (2017) 37–48.

[15] D. Pugh, P. Bowen, R. Marsh, A. Crayford, J. Runyon, S. Morris, A. Valera-Medina, A. Giles, *J. Eng. Gas Turb. Power* 140 (6) (2018) 061502-061502-10.

[16] C. Panoutsos, Y. Hardalupas, A. Taylor, *Combust. Flame* 156 (2) (2009) 273–291.

[17] R. Marsh, J. Runyon, A. Giles, S. Morris, D. Pugh, A. Valera-Medina, P. Bowen, *Proc. Comb. Inst.* 36 (3) (2017) 3949–3958.

[18] British Standard ISO 11042-1:1996, *Gas Turbines. Exhaust Gas Emission Measurement and Evaluation*, British Standards Institution, U.K., 1996.

[19] J. Runyon, R. Marsh, P. Bowen, D. Pugh, A. Giles, S. Morris, *Exp. Therm. Fluid Sci.* 92 (2018) 125–140.

[20] Z. Tian, Y. Li, L. Zhang, P. Glarborg, F. Qi, *Combust. Flame* 156 (7) (2009) 1413–1426.

[21] A.A. Konnov, *Combust. Flame* 156 (11) (2009) 2093–2105.

[22] H. Xiao, M.S. Howard, A. Valera-Medina, S. Dooley, P. Bowen, *Energy Proc.* 105 (2017) 1483–1488.

[23] C.K Law, Combustion Physics, Cambridge University Press, U.K., 2006, pp. 109–113.

[24] T. Rutar, P.C. Malte, *J. Eng. Gas Turb. Power* 124 (4) (2002) 776–783.

[25] N. Syred, *Prog. Energy Combust.* 32 (2006) 93–161.

[26] K. Somarathne, S. Hatakeyama, A. Hayakawa, H. Kobayashi, *Int. J. Hydrogen Energy* 42 (44) (2017) 27388–27399.

[27] A. Hayakawa, T. Goto, R. Mimoto, T. Kudo, H. Kobayashi, *Bull. JSME Mech. Eng. J.* 2 (1) (2015).